We are IntechOpen,
the world's leading publisher of
Open Access books
Built by scientists, for scientists

4,800
Open access books available

122,000
International authors and editors

135M
Downloads

Our authors are among the

154
Countries delivered to

TOP 1%
most cited scientists

12.2%
Contributors from top 500 universities

CLARIVATE ANALYTICS
BOOK CITATION INDEX
INDEXED

WEB OF SCIENCE™

Selection of our books indexed in the Book Citation Index
in Web of Science™ Core Collection (BKCI)

Interested in publishing with us?
Contact book.department@intechopen.com

Numbers displayed above are based on latest data collected.
For more information visit www.intechopen.com

Printed Planar Antenna Designs Based on Metamaterial Unit-Cells for Broadband Wireless Communication Systems

Mohammad Alibakhshikenari,
Mohammad Naser-Moghadasi,
Ramazan Ali Sadeghzadeh, Bal Singh Virdee and
Ernesto Limiti

Additional information is available at the end of the chapter

Abstract

With the continuing development of mobile communications, the communication standards, which include operating frequencies and protocols, are also evolving. In order to accommodate these and future changes, antennas with characteristics of wideband and multiband are becoming a necessity. Hence, wireless communications industries are now demanding broadband antennas that are low-profile and low-volume structures. Conventional planar microstrip antennas are the most common form of printed antennas that have been used for many years. This is because these antennas offer advantages of low cost, conformability, and ease of manufacturing; however, the bandwidth of these types of antennas is highly restricted. Among different types of planar antennas, the slotted structure that offers the simplest structure is compact and radiates omnidirectionally; these features make it an excellent candidate for broadband applications.

Keywords: planar slotted antennas, metamaterials, composite right-/left-handed transmission lines, traveling-wave antenna, wireless communications systems

1. Introduction

Printed planar antennas such as patch antennas are favored over other types of antennas as they are low profile, light weight, and can be easily manufactured using low-cost PCB techniques. These types of antennas are constructed using microstrip integrated circuit technology, where a metal

layer is separated from the ground-plane by a dielectric substrate [1, 2]. The thickness of the metal layer is much smaller than the operating wavelength. Such antennas are conventionally excited through a feed-line with a voltage between the patch and the ground plane. This excites a current on the patch, and hence, a vertical electric field between the patch and the ground plane [3]. The patch element resonates when its width or diameter is near $\lambda_g/2$, leading to relatively large current and field amplitudes, and the radiation mechanism occurs from the fringing fields between the edge of the microstrip and the ground plane. Printed planar antennas essentially radiate energy in a direction perpendicular to the plane of the antenna substrate with moderately high gain [3–5].

The choice of the substrate used is important (dielectric constant, thickness, and loss tangent). There are various shapes of patch antennas (circular being the most common) [4]; however, the principles of operation are essentially the same. Circular patches offer advantages over other geometries for applications such as arrays and can also be easily modified to produce a range of impedance values and radiation patterns.

Microstrip patch antennas enjoy many advantages when compared to other types of antennas; they are relatively small, low profile, low cost, light weight, and can be integrated to other circuits or active devices which can possibly result in a single-board solution, unlike wire, waveguide, or horn antennas for example. This also allows this type of antenna to be easily mounted on objects, such as computers or flying bodies, and can be easily employed for array design.

The most common disadvantage of microstrip antennas is the inherent narrow impedance bandwidth, which is due to the thickness, which is normally thin. The easiest and most well-known method of moderately improving the bandwidth is by increasing the height of the substrate [4], which has the effect of increasing the radiation conductance. However, this is not a desirable option as it leads to introducing surface waves and power loss, but usually works well for bandwidths up to 4–6% [6]. Other disadvantages of microstrip patch patch antenna are low efficiency, low power, and poor polarization purity [5, 7]. To overcome this drawback, various metamaterial (MTM) structures, including split-ring resonator (SRR) [8], spiral, rod, omega, S-shape, and symmetric rings, etc., have been explored in literature [9, 10].

This chapter presents the design and measured performance of compact planar slotted antennas based on unique MTM structures for application in broadband wireless communication systems. Typical realization of MTM transmission line (TL) is based on quasi-lumped TL with elementary cells consisting of a series capacitor and a shunt inductor. In reality, the loss associated with the MTM structure introduces series parasitic inductance in the capacitor, and parasitic shunt capacitance in the inductor; thus, the resulting MTM structure is more accurately represented by a composite right/left-handed (CRLH) transmission-line structure. The optimized "d-shaped" antenna presented in the chapter is shown to operate over a wideband from 0.75 to 4.5 GHz with a peak gain of 3.5 dBi and efficiency of 60% at 2 GHz. Moreover, the antenna is compact and easy to fabricate using standard PCB techniques. In addition, an "X-shaped" antenna, which is also presented here, is shown to operate from 0.4 to 4.7 GHz with a gain of 2 dBi and radiates energy with an efficiency of 65% at 2.5 GHz.

2. Metamaterial traveling-wave antenna

In this section, a traveling-wave planar antenna is implemented using composite right/left-handed structures. The antenna is constructed using a unique metamaterial unit cell implemented by etching "X-shaped" slots inside a rectangular patch. The patch is inductively terminated to the ground plane through a via-hole, as shown in **Figure 1**. The proposed antenna is henceforth referred to as "X-shaped" antenna. The resulting structure displays negative permittivity and permeability characteristics over a given frequency range. The aperture of the antenna can be increased by simply cascading together a number of these metamaterial unit cells, as shown in **Figure 1**. Hence, the antenna's gain and radiation efficiency are improved with negligible effect on its fractional bandwidth, which is contrary to what is observed in traditional antennas.

The antenna was designed and fabricated on Rogers RT/Duroid®5880 substrate, which is a glass microfiber reinforced PTFE composite with dissipation factor $\tan\delta = 0.0009$, dielectric constant $\varepsilon_r = 2.2$, and height $h = 1.6$ mm. The proposed antenna structure essentially acts as a guiding structure for traveling waves; thus, the traveling wave forms the main radiating mechanism. The antenna is excited on the left-hand side at port#1, and is terminated on the right-hand side at port#2 with a matched 50 Ω load, i.e., SMD1206, which is terminated to ground. Surface currents associated with the RF signal travel over the antenna structure in one direction from port#1 to the termination port#2. This is in contrast to conventional standing wave or resonant antennas, such as the monopole or dipole antennas. The nonresonating traveling-wave antenna, shown in **Figure 1**, exhibits a wide operating bandwidth.

The equivalent electrical circuit representing the metamaterial unit cell is shown in **Figure 2(a)**. In the unit cell, the "X-shaped" slot essentially behaves like a series left-handed (LH) capacitance (C_L), and the high impedance stub acts like a shunt LH inductor (L_L). Unavoidable parasitic effects in the unit cell are generated by gaps between patch and ground plane and the current flows over the patch. The parasitic anomalies are represented by the shunt right-handed (RH) capacitance (C_R) and the series RH inductance (L_R). Loss in the structure is modeled by the resistance (R_R, R_L) and conductance (G_R, G_L). Components R_R and G_R represent right-handed loss, and R_L and G_L represent left-handed loss. Important characteristics of the metamaterial unit cell were obtained from the analysis of the loss-less equivalent circuit as described in Ref. [10]. At low frequencies, L_R and C_R can be considered short-circuited and open-circuited, respectively, so that the equivalent circuit can be essentially reduced to a series-C_L/shunt-L_L circuit, which is left-handed since it has antiparallel phase and group velocities. The resulting left-handed circuit has a high-pass nature; therefore, a left-handed stopband is presented below a certain cut-off frequency. At high frequencies, C_L and L_L can be considered as short-circuited and open-circuited, respectively, so that the equivalent circuit can be reduced to the series-L_R/shunt-C_R circuit, which is right-handed since it has parallel phase and group velocities. This left-handed circuit has a low-pass nature; therefore, a right-handed stopband is presented above a certain cut-off frequency. The analysis in Ref. [10] shows that the left-handed structure exhibits negative permeability and permittivity. Unlike conventional or normal right-handed unit cell-based structures, the distinguishing feature of a LH structure is its dimensions; in particular, its length is independent of the guided wavelength, which makes the structure significantly smaller.
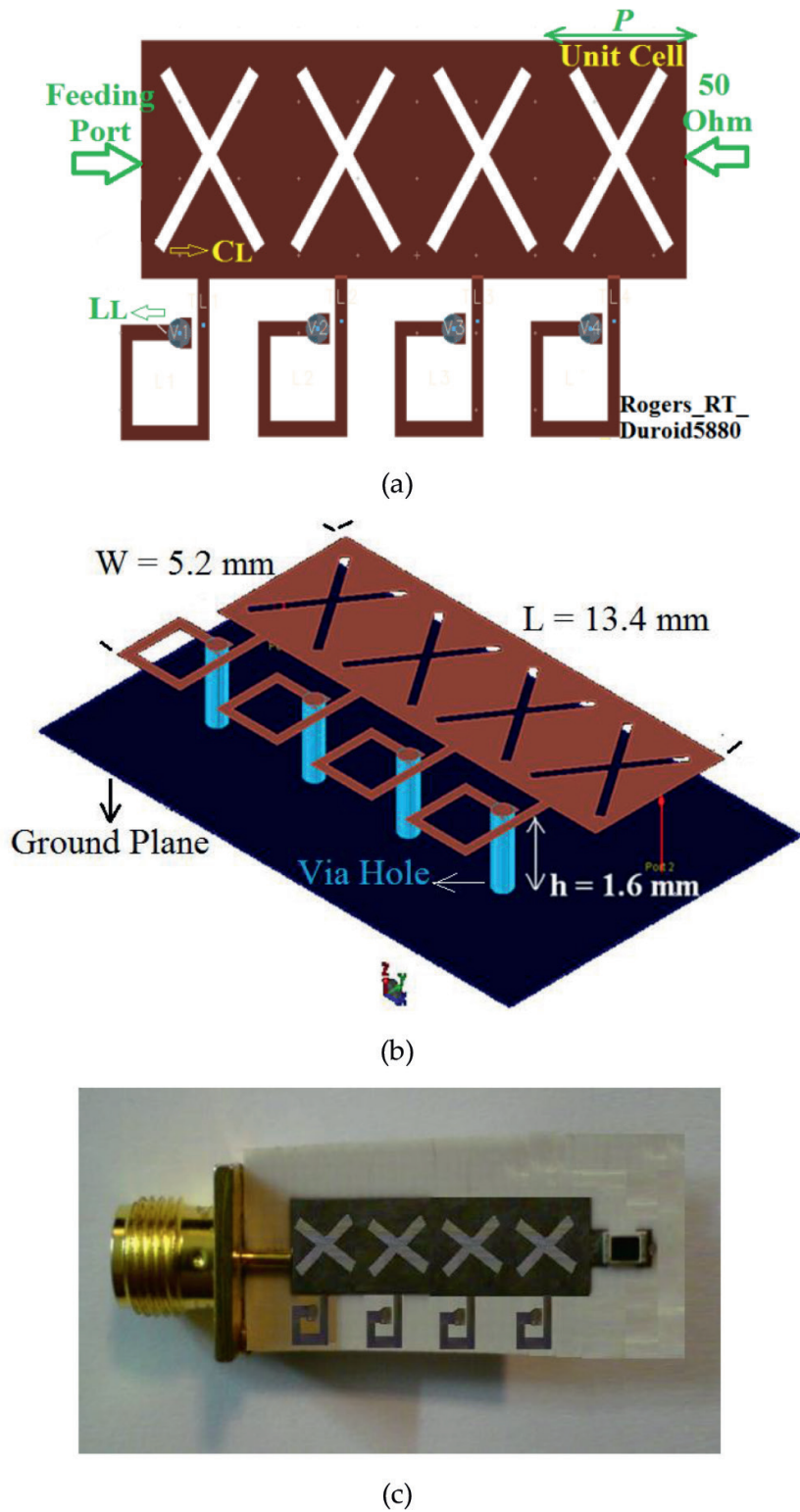
(a)

(b)

(c)

Figure 1. Antenna layout, (a) top layer, (b) isometric view of the simulation model, and (c) the fabricated prototype.

Dispersion diagram of the metamaterial unit cell structure, shown in **Figure 2(b)**, was obtained by substituting the S-parameters, which were obtained with ANSYS HFSS™ (high frequency structure simulator), in Eq.(1) as described in Ref. [10]:
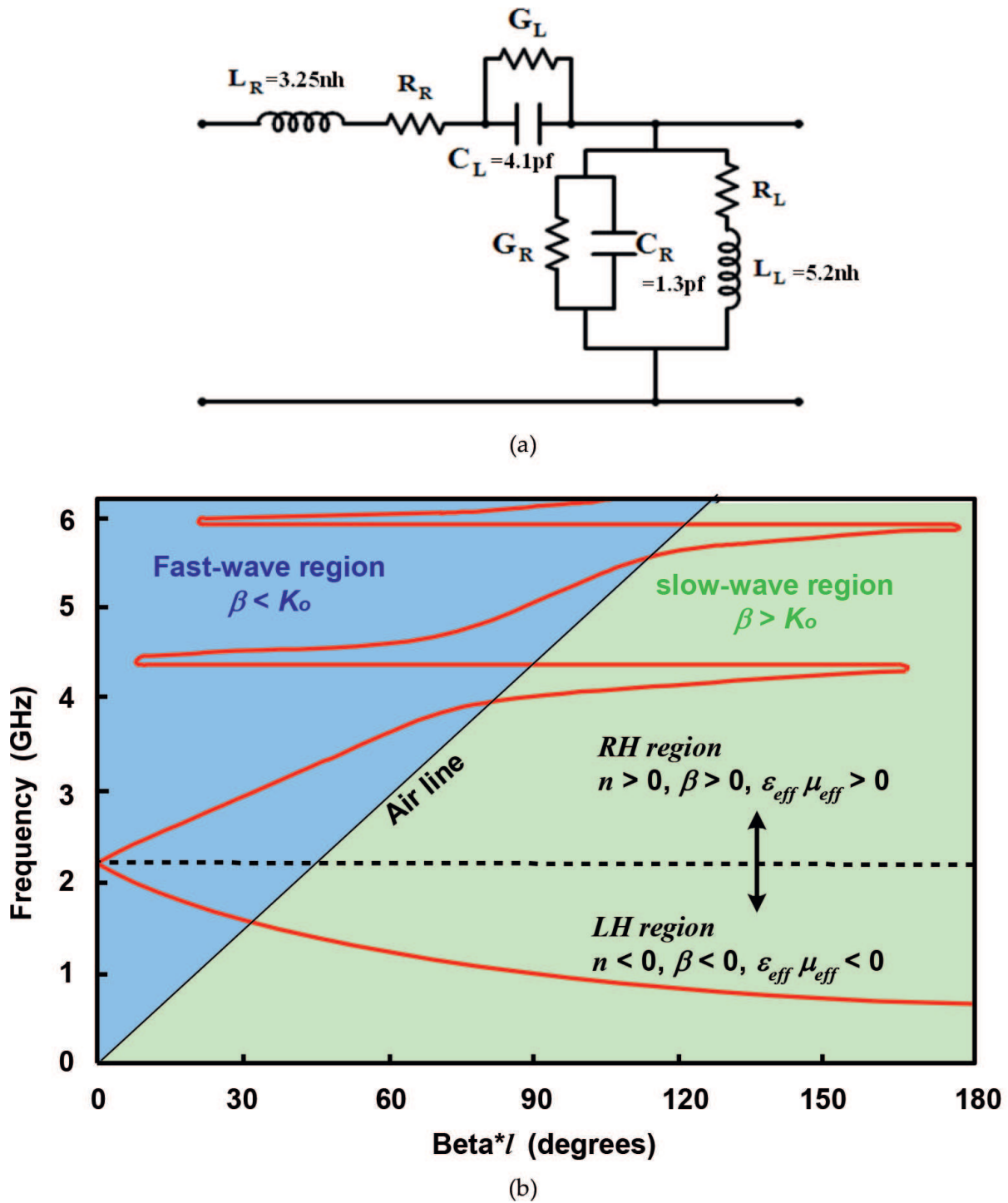
(a)

(b)

Figure 2. (a) Equivalent circuit model of the unit-cell and (b) the dispersion diagram of the loss-less CRLH unit cell.

$$\beta = \cos^{-1}\left(\frac{1 - S_{11} S_{12} + S_{12} S_{21}}{2 S_{21}}\right) / l \qquad (1)$$

The dispersion diagram shows the range of left-handed characteristics (i.e., 0.65–2.25 GHz) and the range of right-handed characteristics (i.e., 2.25–4.4 GHz). The slow-wave and fast-wave regions have been indicated in **Figure 2(b)**. The expression of Air-line, which separates the

fast-wave ($b < K_o$) and slow-wave ($b > K_o$) regions (where K_o is the free-space wave number) is given by:

$$\text{Air-line} = \frac{\omega p}{c} \tag{2}$$

where p is the period of the unit cell as shown in **Figure 1**, and c is the speed of light.

The antenna's characterizing parameters are: $L = 13.4$ mm, $W = 5.2$ mm, $h = 1.6$ mm, $L_R = 3.25$ nH, $C_L = 4.1$ pF, $C_R = 1.3$ pF, and $L_L = 5.2$ nH. These parameters were extracted from the unit cell's simulation model using HFSS™. The prototype microstrip antenna, shown in **Figure 1**(c), was constructed using standard photolithographic techniques. Each of the unit cell has an area of 2.5×5.2 mm^2 ($0.003\lambda_0 \times 0.006\lambda_0$, where λ_0 is free-space wavelength at 400 MHz). Considering the size of SMD1206 (3.4 mm), the overall size of the antenna is $13.4 \times 5.2 \times 1.6$ mm^3 or $0.017\lambda_0 \times 0.006\lambda_0 \times 0.002\lambda_0$.

It is well established that antennas that operate using a resonance configuration have a limited bandwidth that results from destructive interference of the waves. However, by blocking the standing waves and instead using traveling waves can enhance the bandwidth of the antenna as shown below. As mentioned earlier, the proposed antenna provides a guiding structure for traveling waves as the main radiating mechanism. In this configuration, the voltage and current are in phase and have the same $e^{-j\gamma z}$ distribution along the length, where $\gamma = Kz = \beta - j\alpha$. Lower limit of the leaky-wave bandwidth is the frequency at which $\alpha = \beta$ and the upper limit is reached when $\beta = K_o$. In this case, the surface currents that generate the RF signal travel through the antenna in one direction from the input port#1 to the termination port#2, which is in contrast to conventional standing wave or resonant antenna, such as the monopole or dipole. The results presented below confirm that the proposed traveling-wave antenna exhibits a wider operational bandwidth.

Figure 3 shows the simulated and measured reflection-coefficient performance of the traveling-wave antenna. The results reveal that the antenna is particularly sensitive at the following frequencies: 1.4, 2.65, and 3.7 GHz. Simulation results show the antenna has an operating bandwidth of 4.55 GHz from 300 MHz to 4.85 GHz for $S_{11} < -10$ dB. The equivalent fractional bandwidth of the antenna is 176.7%. The measured results show the antenna operates over 400 MHz to 4.7 GHz (for $S_{11} < -10$ dB), which corresponds to a fractional bandwidth of 168.62%. The discrepancy in the simulation and measured results is attributed to manufacturing tolerance and imperfect soldering of the SMA connector.

The measured gain and radiation efficiency of the antenna at various frequencies are tabulated in **Table 1**. The antenna exhibits a maximum gain and radiation efficiency of 2 dBi and 65%, respectively, at 2.5 GHz. The radiation patterns measured in the E-plane and H-plane at 0.4, 1.5, 2.5, and 4.7 GHz are shown in **Figure 4**. These results show that the proposed antenna radiates unidirectionally. It is worth noting that the metamaterial structure which constitutes the antenna has effectively increased the antenna's aperture without increasing its footprint to enhance its gain and radiation characteristics.
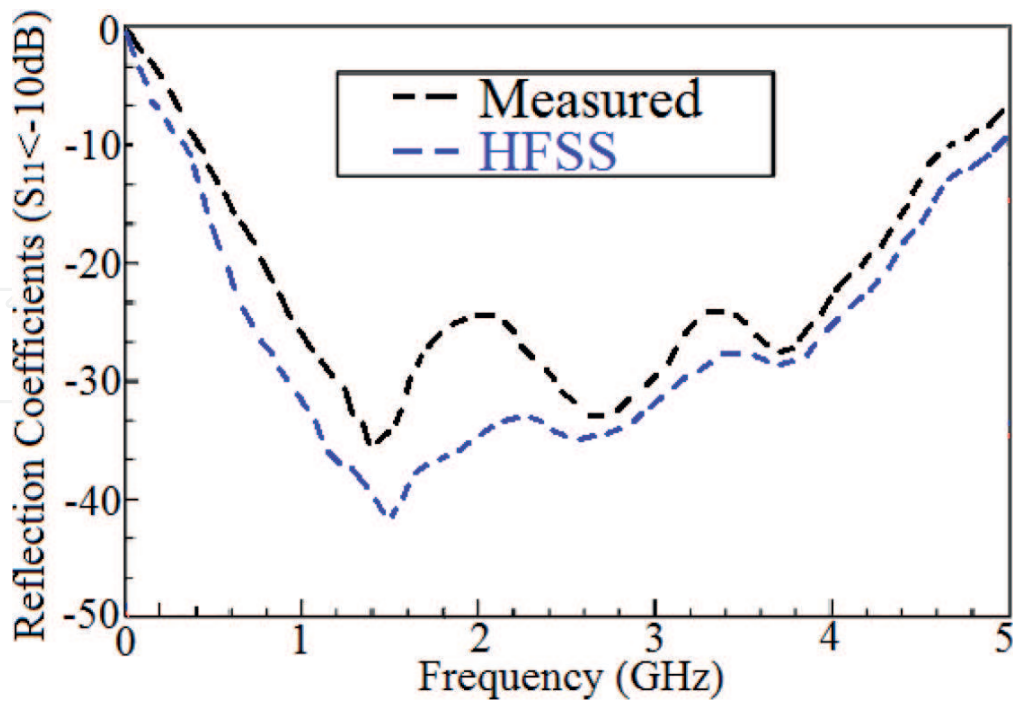
Figure 3. Simulated and measured reflection coefficients response.

Frequency (GHz)	0.4	1.5	2.5	3.5	4.7
Gain (dBi)	0.05	1.5	2	1.5	0.8
Efficiency (%)	8	45	65	42	30

Table 1. Measured gain and radiation efficiency.

This section presented an innovative metamaterial unit cell. The unit cell is easy to implement by simply etching a slot in a patch radiator, which is short-circuited using a high imped- ance line to ground through a via-hole. The proposed antenna is a nonresonant traveling- wave radiator that is significantly smaller than a conventional traveling-wave antenna. This is because the metamaterial antenna's dimensions are independent of frequency. The advan- tages of the proposed antenna are: (i) compactness with a footprint of $13.40 \times 5.20 \times 1.60$ mm^3 ($0.017\lambda_0 \times 0.006\lambda_0 \times 0.002\lambda_0$ at 400 MHz); (ii) low-profile structure; (iii) light weight; (iv) wide- band operation from 400 MHz to 4.7 GHz, which corresponds to a large fractional bandwidth of ~170%; (v) unidirectional radiation patterns in both E-plane and H-plane over its opera- tional frequency bandwidth; and (vi) maximum gain and radiation efficiency of 2 dBi and 65%, respectively, at 2.5 GHz. These characteristics make the antenna attractive for use in multiple wireless communication systems.

The proposed traveling-wave antenna's measured performance is compared with other meta- material and conventional antennas in **Table 2**. It is evident from these results the antenna's operating frequency and fractional bandwidth are superior to metamaterial antennas reported
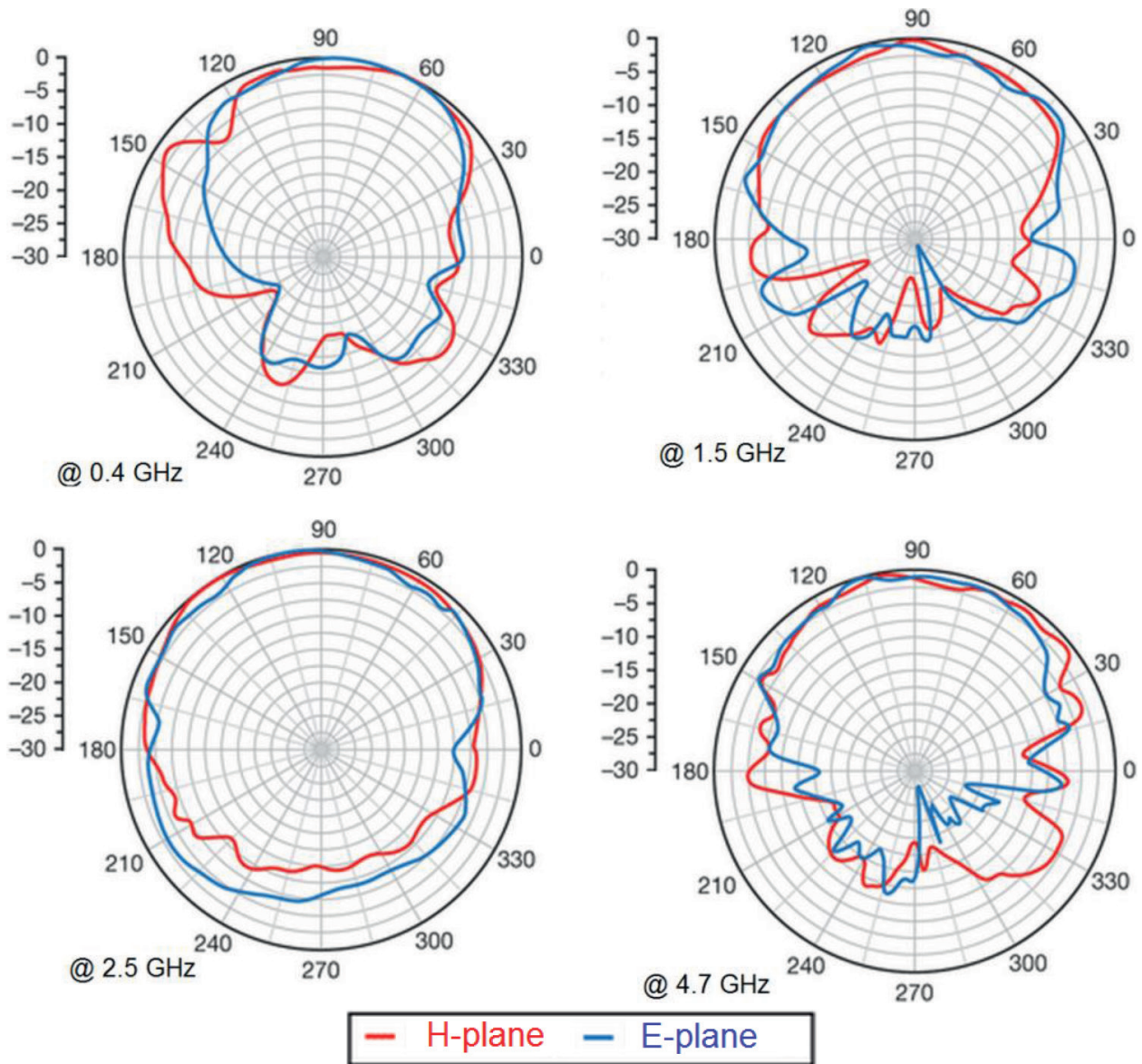
Figure 4. Measured E-plane and H-plane radiation patterns of the proposed antenna.

in Refs. [1, 2]. Its operating frequency band is better than antennas reported in Refs. [1, 2] by a factor of 2.87 and 2.15, respectively; and the fractional bandwidth is better than antennas presented in Refs. [1, 2] by a factor of 7.33 and 4.8, respectively.

To summarize, a novel traveling-wave planar printed antenna is presented in this section based on metamaterial technology. The antenna is shown to provide wideband performance with enhanced gain and radiation efficiency. The low-profile and miniature antenna consists of coupled metamaterial unit cells comprising X-shaped slots and shunted inductive stubs, which are implemented on a rectangular microstrip patch. The proposed antenna is easy to fabricate using conventional PCB manufacturing techniques.

Ref.	Dimensions	Freq. BW/fractional BW	Gain (dBi)	Efficiency (%)
[1]	$20.4 \times 6.8 \times 0.8$ mm^3 $(0.39\lambda_0 \times 0.13\lambda_0 \times 0.015\lambda_0$ @ 5.8 GHz)	5.8–7.3 GHz/23%	4.8	78
[2]	$7.2 \times 5 \times 0.8$ mm^3 $(0.11\lambda_0 \times 0.079\lambda_0 \times 0.012\lambda_0$ @ 4.7 GHz)	4.7–6.7 GHz/35.08%	3.6	60.3
[11]	$12 \times 12 \times 3.33$ mm^3 $(0.09\lambda_0 \times 0.09\lambda_0 \times 0.02\lambda_0$ @ 2.34 GHz)	2.34–2.54 GHz/8.19%	1	20
[12]	$20 \times 25 \times 0.8$ mm^3 $(0.22\lambda_0 \times 0.28\lambda_0 \times 0.009\lambda_0$ @ 3.45 GHz)	3.45–3.75 GHz/8.33%	2	25
[13]	$60 \times 5 \times 5$ mm^3 $(0.16\lambda_0 \times 0.013\lambda_0 \times 0.013\lambda_0$ @ 0.82 GHz)	0.82–2.48 GHz/100.6%	0.45	53.6
This work	$13.4 \times 5.2 \times 1.6$ mm^3 $(0.017\lambda_0 \times 0.006\lambda_0 \times 0.002\lambda_0$ @ 0.4 GHz)	0.4–4.7 GHz/168.62%	2	65

Table 2. Comparison of the metamaterial traveling-wave antenna with other planar antennas (gain and efficiency are optimum values).
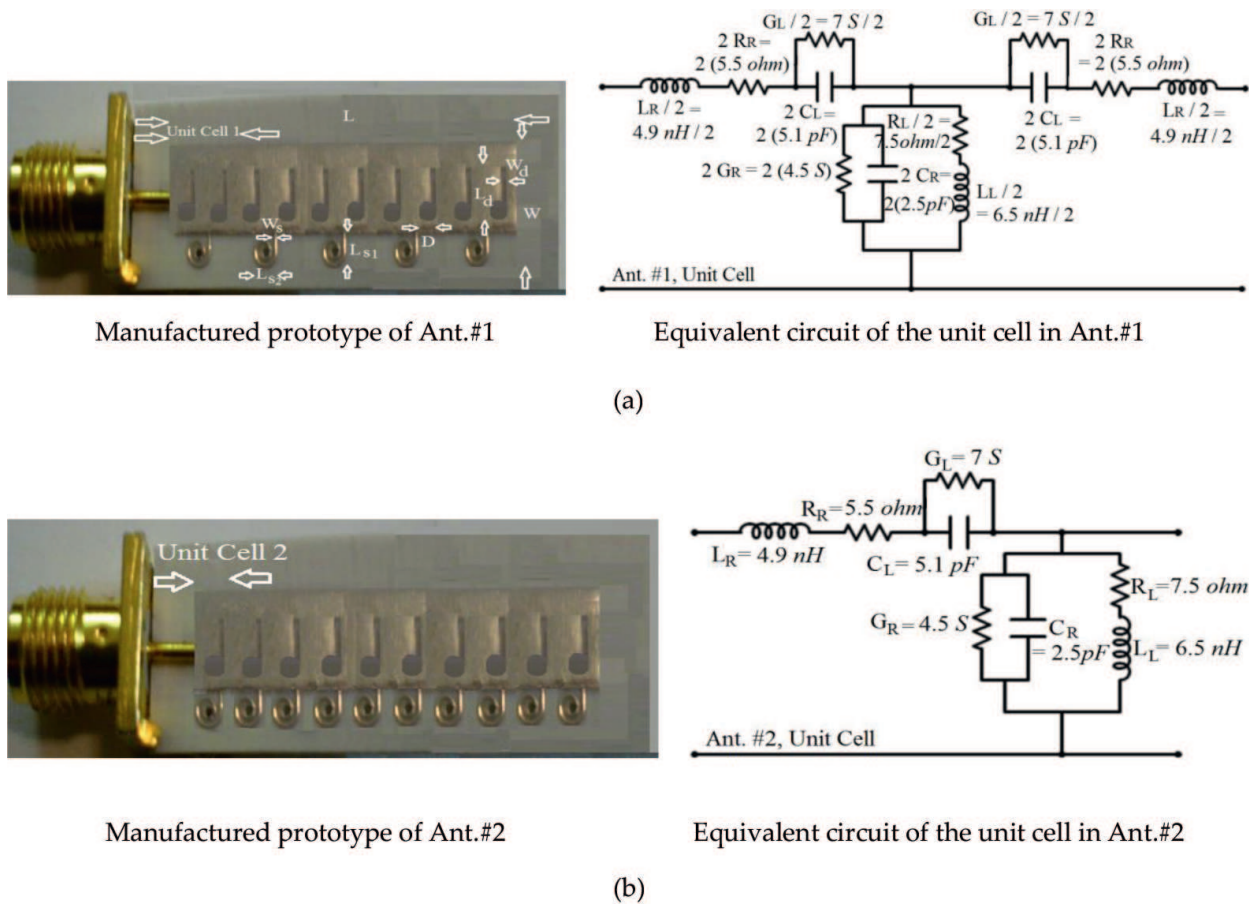
3. Slotted patch antenna

Slotted patch antennas are excellent candidates for broadband applications [9, 14–24]. In this section, a compact planar slotted antenna (PSA) is designed and characterized. The antenna is developed using unique metamaterial structures that can be realized using distributed transmission lines constituted from unit cells consisting of series capacitor and a shunt inductor [1]. As mentioned earlier, in reality, the loss associated with metamaterial structures introduces series parasitic inductance in the capacitor and parasitic shunt capacitance in the inductor. The resulting structure is essentially a composite of right- and left-handed (CRLH) transmission lines [25, 26].

In this chapter, the metamaterial unit cell is realized directly on a patch antenna using a combination of capacitive slot etched on the patch and a short-circuited inductive stub that is realized using a high impedance spiral-shaped transmission line. The proposed antenna is modeled and analyzed using ANSYS HFSS™. The antenna's impedance bandwidth, gain, and radiation efficiency were optimized using HFSS™. In fact, the analysis showed that the antenna's performance can be achieved by simply increasing the number of inductive stubs, which does not affect the antenna's overall size. This is because the metamaterial unit cells in essence increase the aperture of the antenna. The optimized antenna is shown to operate over 0.75–4.5 GHz with a peak gain of 3.5 dBi and radiation efficiency of 60% at 2 GHz. The resulting antenna is highly compact and is fairly easy to manufacture.

The proposed antenna had to operate in the UHF and SHF frequency bands with good radiation characteristics, and had to fit inside an area of 25×10 mm^2. In order to realize these stringent requirements, the antenna was designed using metamaterial unit cells consisting of series left-handed (LH) capacitors and shunt left-handed inductors. The left-handed capacitors

were realized by etching slots on the patch, and the left-handed inductors were realized with a short-circuited high impedance line connected to the patch.

Two antenna prototype designs were evaluated. The first prototype antenna consisted of five unit cells etched on the rectangular patch. Configuration of each unit cell comprised symmetrical arrangement of slot—grounded inductor, where the shape of the slot resembles a crochet note "d," and the inductor is a coiled stub that is grounded through a via-hole. Simulation analysis showed the unusual shape of the slot contributed in enhancing the antenna's performance. **Figure 5** shows the fabricated planar slotted antennas and their equivalent electrical circuit models. Surface currents flowing over the antenna develop a voltage gradient between the metallization and the ground plane to induce parasitic right-handed reactance components, which are represented by the series inductance (L_R) and the shunt capacitance (C_R). Right-handed loss in the structure is represented by R_R and G_R, and left-handed loss by components G_L and R_L. Also included are dielectric loss associated with C_L and the ohmic loss associated with L_L. The planar slotted antenna was implemented on Rogers RO4003® dielectric substrate with permittivity of 3.38, height of 1.60 mm and tanδ of 0.0022. The values of the parameters depicted in **Figure 1** were obtained from HFSS™ analysis, which are: $C_L = 5.10$ pF, $L_L = 6.50$ nH, $C_R = 2.50$ pF, $L_R = 4.90$ nH, $G_L = 7$ S, $G_R = 4.50$ S, $R_L = 7.50$ Ω, and $R_R = 5.50$ Ω.

Manufactured prototype of Ant.#1   Equivalent circuit of the unit cell in Ant.#1

(a)

Manufactured prototype of Ant.#2   Equivalent circuit of the unit cell in Ant.#2

(b)

Figure 5. The two planar slotted antenna configurations. (a) Ant.#1 based on five symmetrical unit cells, (b) Ant.#2 based on 10 asymmetrical unit cells. The size of this antenna is the same as Ant.#1.

Excitation of the antenna through an SMA connector can cause current imbalance resulting in currents flowing over the connector leading to spurious radiation that would degrade the radiation characteristics of the antenna. To prevent this from happening, a second antenna was designed using asymmetrical metamaterial unit cells consisting of slot-grounded inductor configuration, as shown in **Figure 5**(b). The unit cell is constituted from an arrangement of series left-handed capacitor and shunt left-handed inductance. The equivalent electrical model includes loss components represented by R_R, G_R, G_L, R_L, C_L, and L_L. The inductive coils contain the electromagnetic energy near antenna structure and prevent unwanted coupling from happening between the antenna and SMA connector, which helps to enhance the radiation characteristics of the antenna. The antenna's physical and equivalent circuit parameters are given in **Table 3**. The dimensions of antenna and its ground plane size are $25 \times 10 \times 1.60$ mm^3 and 28.50×14.50 mm^2, respectively.

The simulated and measured reflection coefficient performance of the prototype antennas are shown in **Figure 6**. The bandwidth of Ant.#1 is 3.2 GHz for $S_{11} < -10$ dB; however, Ant.#2 provides a wider bandwidth of 3.75 GHz. The gain and radiation efficiency of both antennas in **Figure 7** shows that at 2 GHz, Ant.#1 has a maximum gain and radiation efficiency of 1.5 dBi and 35%, respectively; whereas Ant.#2 performs much better with a maximum gain and radiation efficiency of 3.5 dBi and 60%, respectively. These results show that the antenna's aperture can be increased by simply increasing the number of inductive stubs in the proposed antenna. The discrepancy between the simulated and measured performance in **Figure 6** is prominent at lower frequencies. This is attributed to the feed cable and spurious electromagnetic coupling

UC1	UC2	L_g	W_g	0	L_d	L_{S1}	L_{S2}	W	W_d
5	10	28.50	14.50	25	4	3	1.7	10	0.40
Ws	D	C_L	L_L	C_R	L_R	G_L	G_R	R_L	R_R
0.20	1.40	5.10	6.50	2.50	4.90	7	4.50	7.50	5.50

Table 3. Design parameters (units in mm, pF, nH, S, Ω; unit cell is abbreviated as UC).
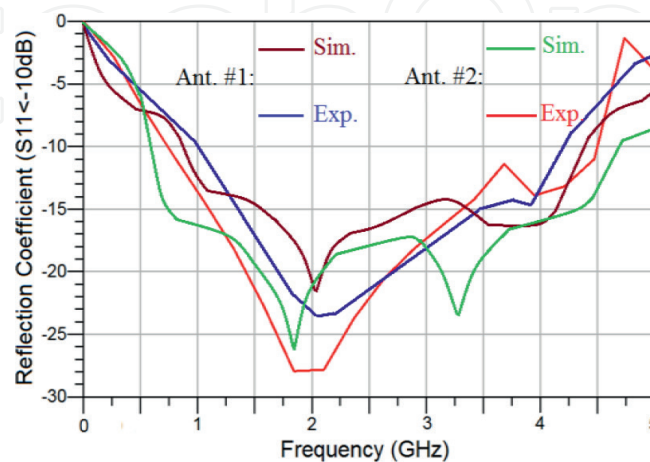
Figure 6. Simulated and measured reflection coefficient response of the two prototype antennas.
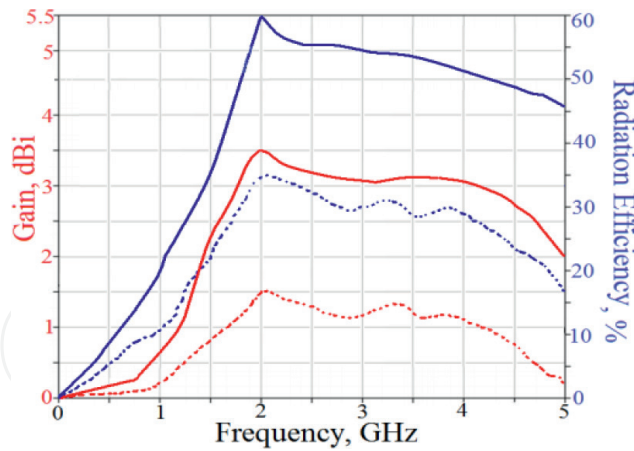
Figure 7. Measured gain and radiation efficiency response of the two prototype antennas. (Ant.#1: dashed lines, and Ant.#2: solid lines).

with the SMA connector. In the simulation, the antenna is excited with a signal source without using a feeding cable. However, in practice, the measurement of the prototype antennas was measured with Agilent's 8722ES vector network analyzer connected to the antenna using a coaxial cable. The salient results are given in **Table 4**.

The measured radiation patterns of Ant.#1 and Ant.#2 in the E-plane and H-plane are shown in **Figure 8**. The radiation pattern of Ant.#1 is predominately bidirectional. At 1 GHz, the E-plane and H-plane radiation patterns of Ant.#1 are analogous to a dipole antenna with a maximum gain at an angle of 180 degrees azimuth; however, at 2 GHz, the maxima gain flips to 0 degrees. At 4 GHz, the maxima gain flips back to at 180 degrees. This phenomenon is observed because of the backward and forward wave variation of the phase with frequency. Ant.#2 exhibits bidirectional radiation patterns in the E-plane and H-plane at 1 GHz; however, the radiation pattern changes to omnidirectional at 2 GHz. The additional inductive stubs essentially suppress the effects of current imbalance over the SMA connector, and hence, improve its impedance bandwidth. At 2 GHz, the radiation gain of Ant.#2 in the H-plane is reduced by about 3 dB at 90 and 270 degrees; and at 4 GHz, a null is observed in the E-plane at 180 degree.

	Ant.#1	Ant.#2	Change
Dimensions	$25 \times 10 \times 1.60$ mm^3 or $0.083\lambda_0 \times 0.033\lambda_0 \times 0.005\lambda_0$ @ 1 GHz Ground-plane of ants.: 28.50×14.50 mm^2 or $0.098\lambda_0 \times 0.048\lambda_0$		None
Bandwidth	Sim.: 0.89–4.33 GHz Fractional BW ≈ 131.8%	Sim.: 0.58–4.7 GHz Fractional BW ≈156.06%	24.26%
	Meas.: 1–4.20 GHz Fractional BW ≈ 123.07%	Meas.: 0.75–4.50 GHz Fractional BW ≈142.85%	19.78%
Gain (dBi)	0.20, 1.50, and 1	0.25, 3.50, and 2.70	2 dB increase @ 2 GHz
Efficiency (%)	11, 35, and 27	13, 60, and 48	25% increase @ 2 GHz

Note: Gain and radiation efficiency were measured at 1, 2, and 4.2 GHz for ant.#1; and at 0.75, 2, and 4.5 GHz for ant.#2.

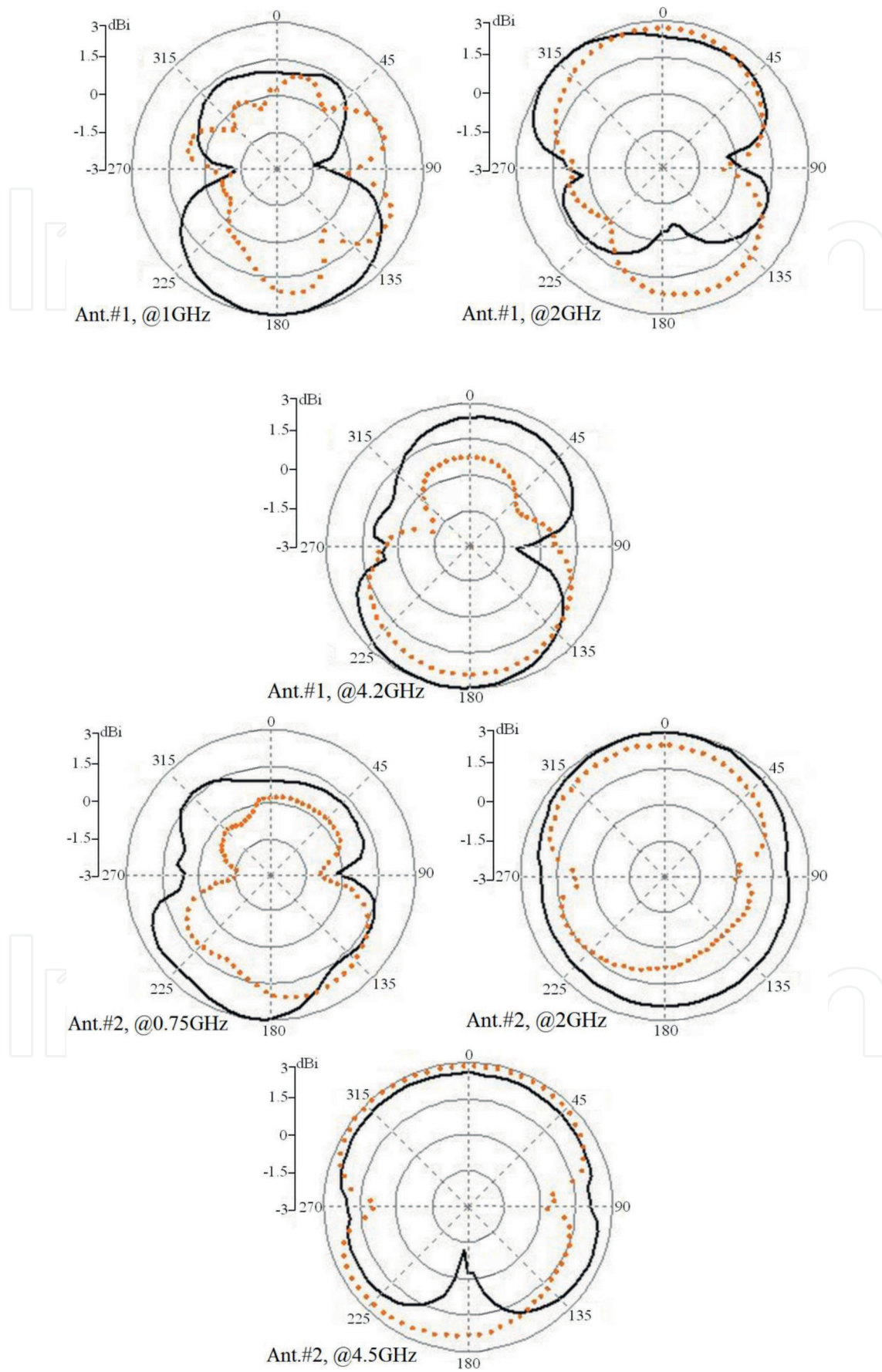**Table 4.** Salient features of the proposed planar slotted antenna.

Figure 8. Measured E-plane and H-plane radiation patterns of Ant.#1 and Ant.#2 at various frequencies.

To summarize, novel planar slotted antenna designs were presented based on metamaterial unit cells that were constituted from capacitive slots etched in the radiating patch and grounded coiled inductive stubs. The fabricated antennas possess the following characteristics: (i) compact structure; (ii) simple layout, which is easy to fabricate at low cost; (iii) low-profile structure that is easy to integrate with RF circuits; and (iv) characteristics suitable for UHF-SHF broadband wireless communication systems.

Author details

Mohammad Alibakhshikenari[1]*, Mohammad Naser-Moghadasi[2], Ramazan Ali Sadeghzadeh[3], Bal Singh Virdee[4] and Ernesto Limiti[1]

*Address all correspondence to: alibakhshikenari@ing.uniroma2.it

1 Department of Electronic Engineering, University of Rome "Tor Vergata", Rome, Italy

2 Faculty of Engineering, Science and Research Branch, Islamic Azad University, Tehran, Iran

3 Faculty of Electrical Engineering, K. N. Toosi University of Technology, Tehran, Iran

4 London Metropolitan University, Center for Communications Technology & Mathematics, London, UK

References

[1] Alibakhshi-Kenari M, Naser-Moghadasi M, Virdee BS, Andújar A, Anguera J. Compact antenna based on a composite right/left handed transmission line. Microwave and Optical Technology Letters. 2015; **57**(8):1785-1788

[2] Alibakhshi-Kenari M. New traveling-wave antenna resonating at 6 GHz based on artificial transmission line metamaterial structures for RF portable devices. Open Journal of Antennas and Propagation. 2013;**1**(2). DOI: 10.4236/ojapr.2013.12003

[3] Collin RE. Field Theory of Guided Waves. 2nd ed. United States: Wiley-Interscience; 1991. chap. 12

[4] Balanis CA. Antenna Theory and Design. United States: John Wiley & Sons; 1997

[5] Pozar DM. Microwave and RF Design of Wireless Systems. New York: John Wiley & Sons, Inc. 2000

[6] Pozar DM. An update on microstrip antenna theory and design including some novel feeding techniques. IEEE Antennas and Propagation Society Newsletter. 1986; **28**(5): 4-9

[7] Bahl IJ, Bhartia P. Microstrip antennas. United States: Artech House; 1980

[8] Alibakhshi-Kenari M, Naser-Moghadasi M, Sadeghzadah RA. Bandwidth and radiation specifications enhancement of monopole antennas loaded with split ring resonators. IET Microwaves, Antennas & Propagation. 2015;**9**(14):1487-1496

[9] Engheta N, Ziolkowski RW editors . Electromagnetic Metamaterials: Physics and Engineering Explorations. Hoboken: Wiley and IEEE Press; 2006

[10] Caloz C, Itoh T. Electromagnetic Metamaterials, Transmission Line Theory and Microwave Applications. Wiley and IEEE Press; 2005

[11] Lee CJ, Leong KM H, Itoh T. Broadband small antenna for portable wireless application. In: International Workshop on Antenna Technology: Small Antennas and Novel Metamaterials; 4-6 March 2008; Chiba, Japan: IEEE; 2008. 10-l3

[12] Yu C-C, Huang M-H, Lin L-K, Chang Y-T. A compact antenna based on MTM for WiMAX. In: Asia-Pacific Microwave Conference; 16-20 December 2008; Macau, China: IEEE; 2008.pp. 1-4

[13] Li Y, Zhang Z, Zheng J, Feng Z. Compact heptaband reconfigurable loop antenna for mobile handset. IEEE Antennas and Wireless Propagation Letters. 2011;**10**:1162-1165

[14] Liu L, Cheung SW, Yuk TI. Bandwidth improvements using ground slots for compact UWB microstrip-fed antennas. Progress in Electromagnetics Research Symposium. 2011;1420-1423

[15] Cheung SW, Liu L, Azim R, Islam MT. A compact circular-ring antenna for ultra-wideband applications. Microwave and Optical Technology Letters. 2011;**53**:2283-2288

[16] Sun YY, Cheung SW, Yuk TI. Studies of Planar Antennas with different radiator shapes for ultra-wideband body-centric wireless communications. Progress in Electromagnetics Research Symposium. 2011:1415-1419

[17] Zhang J, Sun XL, Cheung SW, Yuk TI. CPW-coupled-fed elliptical monopole antenna for UWB applications. IEEE Radio Wireless Week. 2012;295-298

[18] Sun YY, Islam MT, Cheung S W, Yuk TI, Azim T, Misran N. Offset-fed UWB antenna with multi-slotted ground plane. IEEE International Workshop on Antenna Technology. 2011:432-436

[19] Sun YY, Cheung SW, Yuk TI., Planar monopole ultra-wideband antennas with different radiator shapes for body-centric wireless networks. Progress in Electromagnetics Research Symposium. 2012:839-843

[20] Wong H, So KK, Gao X. Bandwidth enhancement of a monopolar patch antenna with V-shaped slot for car-to-car and WLAN communications. IEEE Transactions on Vehicular Technology. 2016;**65**(3):1130-1136

[21] Liu S, Wu W, Fang DG. Single-feed dual-layer dual-band E-shaped and U-slot patch antenna for wireless communication application. IEEE Antennas and Wireless Propagation Letters. 2016;**15**:468-471

[22] Chen J, Tong K-F, Al-Armaghany A, Wang J. A dual-band dual-polarization slot patch antenna for GPS and Wi-Fi applications. IEEE Antennas and Wireless Propagation Letters. 2016;**15**:406-409

[23] Cao W-Q, Hong W, Cai Y. Microstrip-line-slot fed EDPA elements and array with ELP. IET Microwaves, Antennas & Propagation. 2016; **10**(12):1304-1311

[24] Soltanpour M, Fakharian MM. Compact filtering slot antenna with frequency agility for Wi-Fi/LTE mobile applications. Electronics Letters. 2016;**52**(7):491-492

[25] Eleftheriades GV. EM transmission-line metamaterials. Materials Today. 2009;**12**(3):30-41

[26] Lai A, Caloz C, Itoh T. Composite right/left handed transmission line metamaterials. IEEE Microwave Magazine. 2004;**5**(3):34-50